



# Bioinformatics analysis of microenvironment-related genes associated with radioresistance in glioblastoma

Yun Liu<sup>1</sup>, Yufei Zhao<sup>1</sup>, Jinmei Fang<sup>1</sup>, Jing Fang<sup>1</sup>, Xiaodong Yuan<sup>2</sup>

<sup>1</sup>Department of Radiation Oncology, Anhui Provincial Cancer Hospital, The First Affiliated Hospital of USTC, Division of Life Sciences and Medicine, University of Science and Technology of China, Hefei, China; <sup>2</sup>Organ Transplant Center, The First Affiliated Hospital of USTC, Division of Life Sciences and Medicine, University of Science and Technology of China, Hefei, China

**Contributions:** (I) Conception and design: Y Liu, X Yuan; (II) Administrative support: Y Zhao, X Yuan; (III) Provision of study materials or patients: X Yuan, Y Zhao; (IV) Collection and assembly of data: Y Liu, J Fang, J Fang; (V) Data analysis and interpretation: Y Liu, X Yuan; (VI) Manuscript writing: All authors; (VII) Final approval of manuscript: All authors.

**Correspondence to:** Xiaodong Yuan. Organ Transplant Center, The First Affiliated Hospital of USTC, Division of Life Sciences and Medicine, University of Science and Technology of China, Hefei 230036, China. Email: docyuan@ustc.edu.cn.

**Background:** Immune and stromal cells are the two major non-tumor cell types in the glioblastoma (GBM) microenvironment, which play critical roles in the prognostic assessment of tumors. Previous findings have identified genes with prognostic value in the GBM microenvironment; however, correlations between microenvironment-related genes and GBM radioresistance remain unclear. Therefore, in this study, we screened for vital microenvironment-related genes associated with radioresistance in GBM.

**Methods:** We analyzed the data from 348 patients with primary GBM that had undergone radiotherapy (patients with GBM-RT), in The Cancer Genome Atlas database. The Estimation of STromal and Immune cells in Malignant Tumor tissues using Expression data (ESTIMATE) algorithm was used to calculate stromal and immune scores to identify the differentially expressed genes (DEGs). Functional enrichment analyses and a protein-protein interaction (PPI) network construction were performed. Survival analysis was conducted to determine genes with prognostic value. The Chinese Glioma Genome Atlas (CGGA) cohort was utilized for validation.

**Results:** The stromal score was significantly correlated with the prognoses of patients with GBM-RT. Based on the stromal and immune scores, 139 common DEGs involved in inflammation or immune-related activities were identified. We also identified 86 DEGs associated with poor prognosis, which further intersected with the top nodes in the PPI network. Finally, we identified the shared DEGs using the CGGA database and found 10 genes with prognostic value that contributed to GBM radioresistance. These genes included *TLR2*, *C3AR1*, *CD163*, *ALOX5AP*, *NCF2*, *CYBB*, *FCGR1A*, *FCGR2A*, *FCGR2B*, and *RNASE6*.

**Conclusions:** We identified several genes related to the immune microenvironment that may mediate GBM radioresistance. Our findings provide a theoretical basis for predicting the radioresponse and survival of patients with GBM.

**Keywords:** Estimation of STromal and Immune cells in Malignant Tumor tissues using Expression data (ESTIMATE); tumor microenvironment; radioresistance; glioblastoma (GBM)

Submitted Jul 06, 2020. Accepted for publication Oct 26, 2020.

doi: 10.21037/tcr-20-2476

View this article at: <http://dx.doi.org/10.21037/tcr-20-2476>

## Introduction

Glioblastoma (GBM) is the most common primary brain tumor in adults, and has a high rate of mortality. Despite

improvements in therapeutic strategies, its clinical outcomes remain poor, with a median survival time of approximately 15 months (1). GBM cells exhibit aggressive behavior,

with high levels of invasion and diffuse infiltration into the surrounding brain parenchyma, which makes complete tumor resection impossible (2). Radiotherapy (RT) is an effective treatment modality for eliminating residual tumor cells. Unfortunately, most patients with GBM experience local recurrence at the original lesion sites where high doses of radiation were delivered, confirming the radioresistance of GBM (3). To further improve the efficacy of RT, the underlying mechanism of GBM radioresistance should be determined, and biomarkers for assessing treatment responses and prognosis must be identified.

GBM cells coexist with non-tumor cells in a dynamic microenvironment, which promotes GBM proliferation, invasion, and survival. Numerous studies have shown that the intrinsic characteristics of GBM cells as well as their interactions with the microenvironment contribute towards GBM resistance to RT (4). The GBM microenvironment contains a diverse array of non-tumor cells, including immune cells, stromal cells, and endothelial cells, as well as extracellular matrix components. The two major types of cells in the GBM microenvironment are infiltrating immune cells (such as microglia, macrophages, lymphocytes, neutrophils, and dendritic cells) and stromal cells (such as neurons, astrocytes, and oligodendroglia) (5). Several findings have demonstrated the critical roles of immune and stromal cells in the prognostic assessment of tumors.

Using public databases and novel biological algorithms that provide survival estimates for patients, considerable progress has been made in predicting cancer prognosis based on clinical features and gene-expression profiles (6). The recently developed Estimation of STromal and Immune cells in Malignant Tumor tissues using Expression data (ESTIMATE) algorithm can be used to evaluate stromal and immune scores, and to predict the infiltration of non-tumor cells based on their unique gene-expression signatures (7). The ESTIMATE algorithm has been applied for predicting prognosis and for identifying genetic alterations in many cancers, including GBM (8-10). Although Jia *et al.* identified genes with prognostic value in the GBM microenvironment, the relationship between microenvironment-related genes and GBM radioresistance is unclear (8). Thus, immune and stromal scores can be used to assess the radioresponse of GBM from a genome-wide perspective.

Here, we evaluated the associations between immune and stromal scores, and the clinical outcomes of patients with GBM undergoing RT (GBM-RT), using data from The Cancer Genome Atlas (TCGA) database and the ESTIMATE algorithm. We identified microenvironment-

related genes that correlated with radioresistance and a poor prognosis for GBM, which were validated using data from the Chinese Glioma Genome Atlas (CGGA) cohort. Understanding the relationship between the immune microenvironment and GBM radiosensitivity may aid the development of strategies to improve the efficacy of RT.

We present the following article in accordance with the MDAR reporting checklist (available at <http://dx.doi.org/10.21037/tcr-20-2476>).

## Methods

### Databases

The RNA-sequencing (RNA-seq) data and clinical information for patients with primary GBM, including 348 patients who underwent RT treatment and had detailed survival-time records, were retrieved from TCGA (<https://tcga-data.nci.nih.gov/tcga/>). For the validation cohort, RNA-seq data and clinical information for patients with primary GBM, including 71 patients who underwent RT treatment and had detailed survival-time records, were extracted from the CGGA (<http://www.cgga.org.cn/>). The ESTIMATE algorithm was used to evaluate the proportion of non-tumor components in the tumor microenvironment according to their gene-expression signatures, which are represented by the ImmuneScore, StromalScore, and ESTIMATEScore (7). The ImmuneScore and StromalScore of TCGA GBM cases were available from a public source website (<https://bioinformatics.mdanderson.org/estimate/>). The study was conducted in accordance with the Declaration of Helsinki (as revised in 2013).

### Identification of differentially expressed genes (DEGs)

The limma package of R software was utilized to identify DEGs by comparing the high-score and low-score cases (11). Gene-expression levels with a  $|\log_2(\text{fold-change})|$  score of  $>1$  and an adjusted (adj.) P value of  $<0.05$  were considered significantly different.

### Heatmaps, volcano plots, and Venn diagrams

Heatmaps of DEGs were constructed using the ClustVis web tool (<https://biit.cs.ut.ee/clustvis/>), and volcano plots for DEGs were generated with GraphPad Prism. DEGs common to different groups were identified by generating Venn diagrams, which were created using an online analysis tool

(<https://bioinfo.cnb.csic.es/tools/venny/index.html>) (12).

### ***Enrichment analysis of Gene Ontology (GO) and Kyoto Encyclopedia of Genes and Genomes (KEGG)***

The clusterProfiler, org.Hs.eg.db, enrichplot, and ggplot2 packages of R software were used to perform GO and KEGG enrichment analysis of DEGs. GO categories were analyzed, including biological processes (BPs), molecular functions (MFs), and cellular components (CCs). Categories with P and q values of <0.05 were regarded as being significantly enriched.

### ***Protein-protein interaction (PPI) network construction***

The PPI network of the common DEGs was generated using the STRING database (<http://string-db.org>) (13). An interaction score of  $\geq 0.4$  was selected as the cutoff criterion. PPI network data were reconstructed using Cytoscape software to identify genes and to perform module analysis. Molecular Complex Detection was applied to detect the clusters in the network, and individual networks with more than 10 nodes were included.

### ***Statistical analysis***

Statistical analyses were conducted using R software (version 4.0.0) and GraphPad Prism (version 7.0.0; GraphPad, Inc., La Jolla, CA, USA). Data for 348 patients with primary GBM (TCGA GBM database) were assigned high or low immune and stromal scores relative to the median ImmuneScore and StromalScore, respectively. Individual DEGs were grouped as having high or low expression relative to the median score of each individual gene-expression value. The Kaplan-Meier method was used for survival analysis and  $P < 0.05$  (determined with the log-rank test) was regarded as reflecting a statistically significant difference. To determine the prognostic values of DEGs, the survival package of R software was used for univariate Cox regression analysis, and  $P < 0.05$  was considered a significant difference.

### ***Workflow***

The workflow of the current study is shown in [Figure S1](#). RNA-seq data and clinical information for 539 patients were downloaded from TCGA database, of which 348 cases undergoing RT were included in this study. ESTIMATE

scores, including stromal and immune scores, were obtained using the gene expression data from GBM tumor tissues. The impact of ESTIMATE scores on the prognosis of patients with GBM-RT was investigated. Shared DEGs were obtained by intersection analysis between the PPI network and univariate Cox regression analyses. DEGs with prognostic value for RT were further validated using the CGGA GBM database.

## **Results**

### ***Tumor stromal and immune scores correlated with the clinical outcomes of patients with GBM-RT***

To investigate correlations between the overall survival (OS) of patients with GBM-RT and their stromal/immune scores, TCGA data from 348 patients with GBM-RT were obtained and divided into high and low groups (RT<sup>+</sup> stromal score<sup>high</sup>, RT<sup>+</sup> stromal score<sup>low</sup>, RT<sup>+</sup> immune score<sup>high</sup>, and RT<sup>+</sup> immune score<sup>low</sup> groups), based on their stromal and immune scores. The median values of the stromal and immune scores were 84.5 and 966.78, respectively. Survival curves showed that patients with high stromal scores had a shorter OS than those with low stromal scores (*Figure 1A*,  $P = 0.0166$ ; log-rank test) and that patients with high immune scores tended to have a shorter median OS (*Figure 1B*,  $P = 0.0661$ ; log-rank test). These results indicate that the stromal or immune score plays a role in determining the clinical outcomes of patients with GBM-RT. Moreover, the stromal score showed greater prognostic value than the immune score and was more suitable for stratifying the radioresponses of patients with GBM.

### ***Associations between gene-expression profiles and stromal and immune scores***

To determine the gene expression profiles, differential analysis of 348 patients with GBM-RT was performed according to the stromal or immune scores. DEGs were identified using a threshold of  $|\log_2(\text{fold-change})| > 1$  and an adj. P value of <0.05. We identified 168 and 205 DEGs that were upregulated in the high-stromal score and high-immune score groups, respectively (*Figure 1C,D*, [Figure S2A,B](#)). Venn diagrams were used to identify critical genes relevant to the GBM microenvironment; 139 upregulated DEGs overlapped with the high-stromal and high-immune score groups, whereas 13 downregulated DEGs were identified

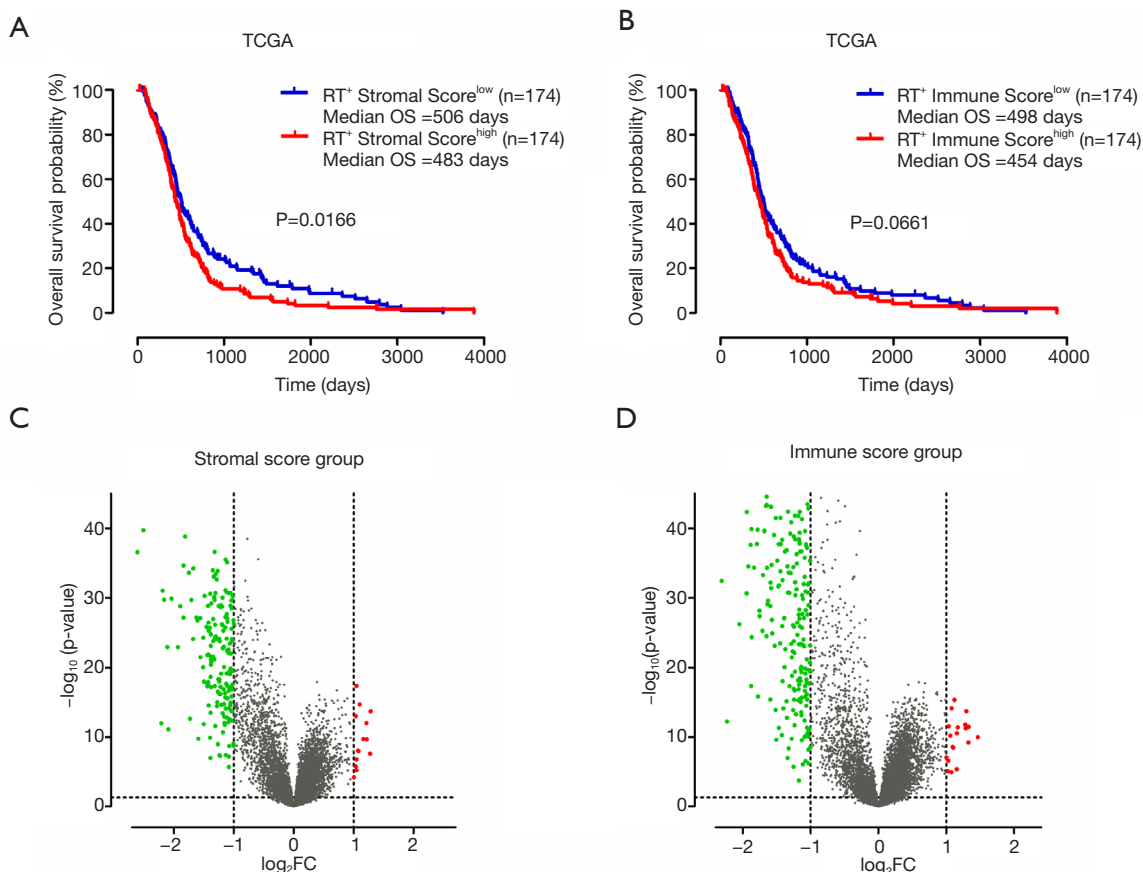


**Figure 1** Correlation of stromal and immune scores with the survival of patients with GBM undergoing RT. (A) Kaplan-Meier survival analysis of patients with GBM-RT and high or low stromal scores relative to the median stromal score;  $P=0.0166$ , as determined by the log-rank test. (B) Kaplan-Meier survival analysis of patients with GBM-RT in high or low immune scores relative to the median immune score;  $P=0.0661$ , as determined by the log-rank test. (C,D) Volcano plots of DEGs generated by comparing groups with high or low stromal scores (C), and high or low immune scores (D). Green and red dots indicate the upregulated genes in patients with high and low scores, respectively. OS, overall survival in terms of days; GBM, glioblastoma; GBM-RT, GBM undergoing radiotherapy; DEG, differentially expressed gene.

(Figure S2C,D).

#### Functional enrichment analysis of DEGs in patients with GBM-RT

To analyze the underlying biological functions of DEGs, functional enrichment clustering of the 139 shared DEGs was performed. We identified 359, 36, and 62 GO terms representing BPs, MFs, and CCs, respectively, that were significantly enriched (Figure 2A,B, Figure S3, and Tables S1-S3;  $q < 0.05$  and adj.  $P < 0.05$ ). The top GO terms included antigen processing and presentation, response to interferon-gamma, major histocompatibility complex (MHC) class

II protein complex, peptide antigen binding, and immune receptor activity. KEGG analysis revealed enrichment of 56 pathways ( $q < 0.05$  and adj.  $P < 0.05$ ) involved in various aspects of inflammation and immunity, including *Staphylococcus aureus* infection, inflammatory bowel disease, the IL-17 signaling pathway, NF- $\kappa$ B signaling pathway, TNF signaling pathway, cytokine-cytokine receptor interaction, and Toll-like receptor signaling pathway (Figure 2C,D, Table S4). The results demonstrate that the biological functions of the DEGs were linked to inflammation or immune-related activities, indicating that inflammation or immune features in the GBM microenvironment mediate GBM radioresistance.

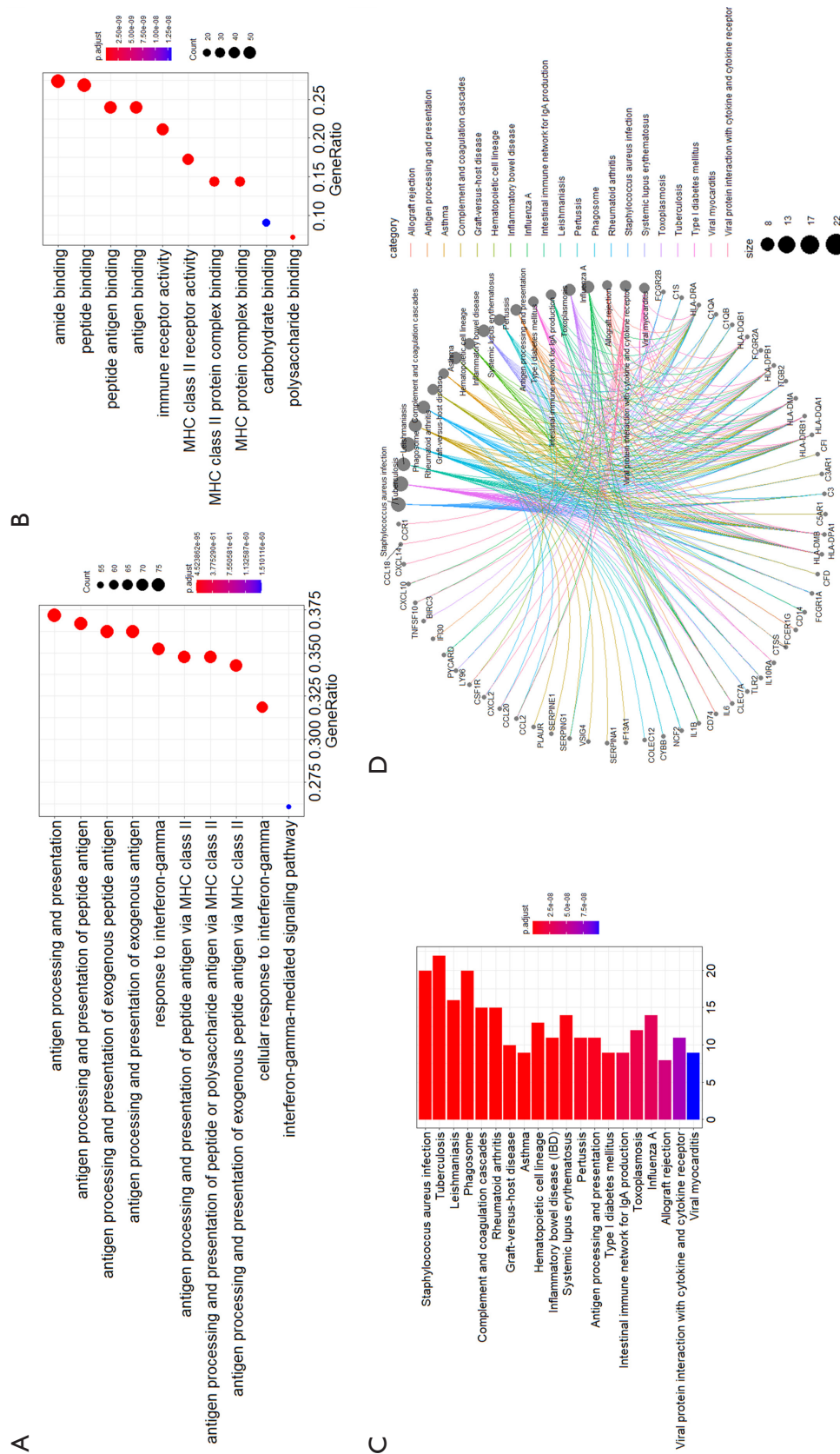


**Figure 2** Functional enrichment analysis. (A,B,C) GO enrichment analysis of 139 DEGs in terms of biological processes (A) and molecular functions (B). Bubble diagram showing the top 10 over-represented GO terms. (C) KEGG pathway-based analysis of 139 DEGs. The bar chart shows the top 20 over-represented KEGG pathways. (D) Cnetplot of KEGG-signal pathways showing the “pathway-gene” network. GO, Gene Ontology; DEG, differentially expressed gene; KEGG, Kyoto Encyclopedia of Genes and Genomes.

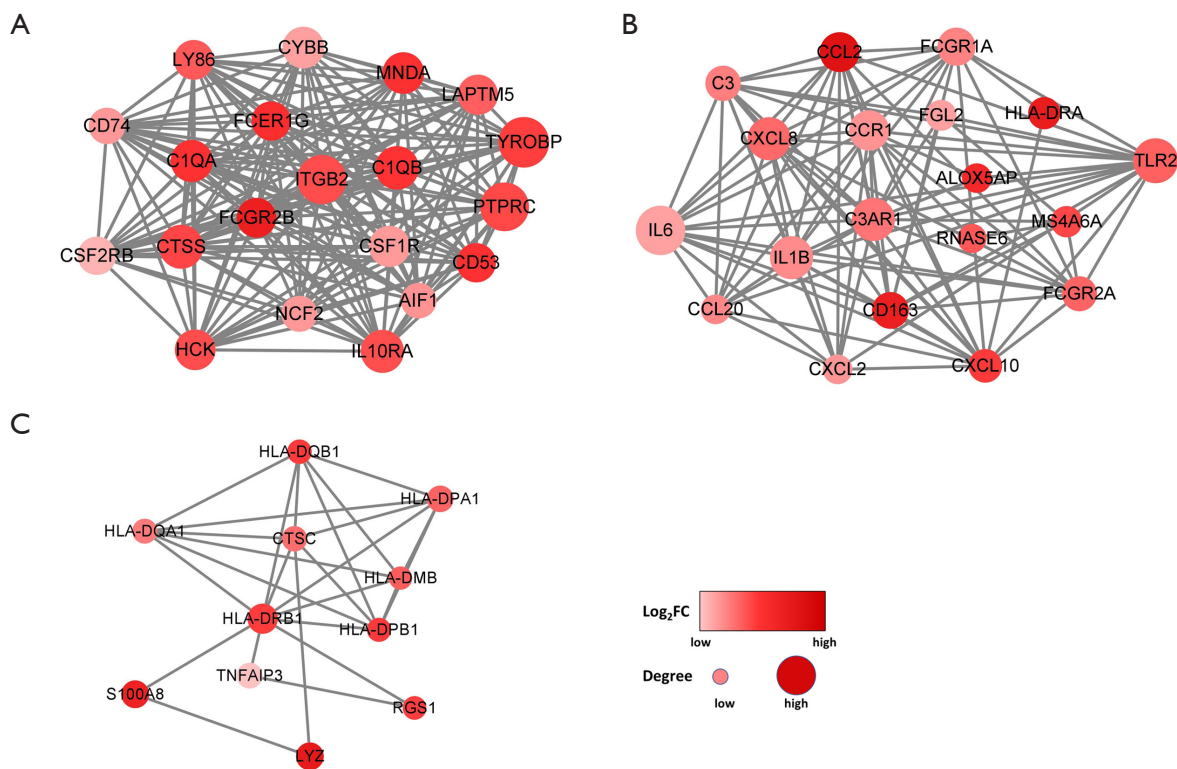


**Figure 3** PPI network and hub genes. The top three PPI networks of DEGs are shown. A combined interaction score with a value of more than 0.4 was regarded as reflecting a significant difference. Log<sub>2</sub> fold-changes are represented by the colors of the nodes, and interactions among proteins are represented by the sizes of nodes. PPI, protein-protein interaction; DEG, differentially expressed gene.

### PPIs among genes with radioresistance signatures

A PPI network was created to investigate the roles of the identified DEGs in GBM radioresistance. The network included 132 nodes and 1,357 edges, and consisted of three significant modules, based on the results of the Molecular Complex Detection method. The representative nodes were TYROBP (Figure 3A), IL-6 (Figure 3B), and HLA-DRB1 (Figure 3C), which were closely connected with other nodes in each module.

### Identification of prognostic DEGs in patients with GBM-RT

Next, Cox regression analysis was conducted to investigate the roles of identified DEGs in the prognosis of patients with GBM-RT. A total of 88 DEGs (86 and 2 shared DEGs upregulated in the high- and low-expression stromal and immune groups, respectively) were shown to significantly correlate with the OS of patients with GBM-RT (Table S5;  $P < 0.05$ ). Furthermore, 29 DEGs were obtained by

overlapping the top nodes in the PPI network, and 86 significant DEGs were identified by Cox regression. Among the 29 overlapping genes, log-rank tests and Kaplan-Meier plots indicated that 19 genes had prognostic value in patients with GBM-RT (Figure 4A,B,C,D and Figure S4) and were associated with a poor response to RT.

### Validation of DEGs using the CGGA database

To determine whether the DEGs in TCGA database had prognostic significance in other cases of GBM, the 19 genes were further investigated using data from the CGGA database. The gene-expression data of 325 patients with glioma, including 71 with GBM-RT, were downloaded and analyzed. We found that 10 of the 19 genes were significantly linked to a poor prognosis in patients with GBM-RT in the CGGA cohort, according to the log-rank test. These genes included *TLR2*, *C3AR1*, *CD163*, *ALOX5AP*, *NCF2*, *CYBB*, *FCGR1A*, *FCGR2A*, *FCGR2B*, and *RNASE6*. The Kaplan-Meier plots of all 10 genes are shown in Figure 4E,F,G,H and Figure S5.

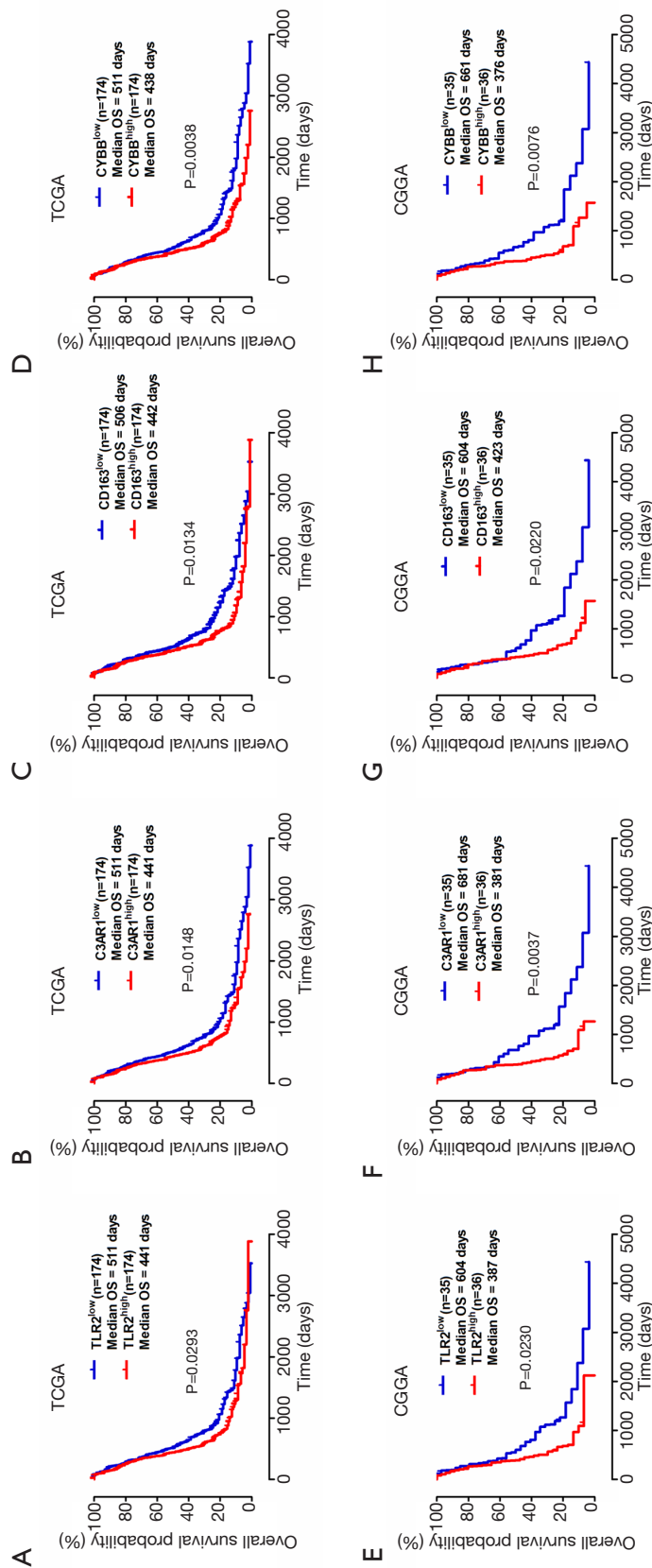


**Figure 4** Correlation of the selected DEGs with the OS of patients in TCGA and the CGGA databases. (A,B,C,D) Correlation of selected DEGs with OS of patients in TCGA database. (E,F,G,H) Validation of the selected DEGs by studying the OS of patients in the CGGA database. Survival analysis was conducted by generating Kaplan-Meier curves. DEGs were grouped based on high (red line) or low (blue line) expression levels relative to the median gene-expression level. P<0.05, as determined by the log-rank test. OS, overall survival in terms of days; DEG, differentially expressed gene; TCGA, The Cancer Genome Atlas; CGGA, Chinese Glioma Genome Atlas.

## Discussion

Radioresistance is considered the main cause of early recurrence and unsatisfactory clinical outcomes in patients with GBM. Thus, exploring the molecular basis of radioresistance is essential for improving the efficacy of RT in GBM management. The interplay between RT and the GBM microenvironment is reported to contribute to radioresistance development (14). Of the various stromal cells in the microenvironment, astrocytes interact most frequently with GBM cells to mediate the radioresponse (15). With respect to immune cells, macrophages and microglia in the microenvironment induce stemness and chemoradioresistance in GBM cells (16). Additionally, changes in the GBM microenvironment induced by RT can in turn contribute to radioresistance, leading to tumor relapse (17).

We identified the GBM microenvironment-related genes in TCGA database that appeared to contribute to GBM radioresistance, and verified the gene signature using the CGGA database. First, we determined the stromal and immune scores, and investigated their relationships with the prognoses of patients with GBM-RT. Notably, a previous report revealed no significant correlation between OS and the immune and stromal scores of patients with GBM (8). In contrast, our results indicated that higher stromal scores were significantly correlated with a shorter OS in patients with GBM-RT, suggesting that the stromal score is a negative prognostic indicator that can be used to predict the radioresponses of patients with GBM. Next, we established the global-expression profiles of genes in the GBM microenvironment, according to the stromal or immune scores. Functional enrichment analyses indicated that these genes participated in inflammation and immune activities, suggesting that immune features in the GBM microenvironment play vital roles in mediating GBM radioresistance. PPI-network analysis revealed that 19 DEGs had prognostic value and were associated with radioresistance. To confirm the validity and reliability of these results, these genes were further validated using data from the CGGA cohort. Finally, 10 DEGs were found to be significantly related to the poor prognosis of patients with GBM-RT and to radioresistance. Three of these DEGs including *CD163*, *TLR2*, and *C3AR1* have been reported to play potential roles in the resistance of tumor cells to RT.

*CD163* is a marker of tumor-associated macrophages. Increasing evidence has revealed that accumulation of *CD163*-positive tumor-associated macrophages plays

important roles in tumor invasion, progression, and poor clinical outcomes in patients with breast cancer (18) and nasopharyngeal carcinoma (19). In the case of breast cancer, patients with *CD163*-positive tumors had a shorter OS following postoperative RT, suggesting that *CD163* is involved in radioresistance. This possibility was confirmed by conducting *in vitro* experiments (20). Additionally, *CD163* was also reported to be overexpressed in glioma cells and to contribute to an unfavorable prognosis in patients with GBM (21). Notably, *CD163* is a specific marker of M2 macrophages in patients with GBM (22), and is known to be involved in GBM radioresistance (23). *TLR2* is a member of the TLR family, which comprises critical modulators of the innate immune responses to pathogen- and damage-associated molecules. *TLR2* overexpression is known to be related to increased risks of tumorigenesis and poor outcomes in patients with gastric cancer (24), prostate cancer (25), and colon cancer (26). In a murine model of orthotopic glioma, *TLR2* activation of microglia promoted glioma immune-system evasion (27). Consistent with our results, Li *et al.* showed that *TLR2* was positively associated with the glioma grade and poor OS, and that *TLR2* overexpression contributed to glioma progression (28). Notably, radioresistant effects of *TLR2* were also demonstrated. *In vivo* experiments showed that *TLR2*-knockout mice were more susceptible to irradiation-induced death, whereas treatment with the *TLR2*-ligand Pam3CSK4 induced radioresistance (29). However, *TLR2* activation has also been reported to play a role in innate and adaptive immunity against brain tumors (30). Thus, the specific relationship between *TLR2* and both GBM tumor progression and radioresistance requires further investigation. *C3AR1* encodes the complement C3a receptor 1 (*C3aR1*), a complement cascade receptor that functions as an immune regulator. Findings with experimental tumor models have indicated that signaling through *C3aR1* can impact tumor growth by modifying immune infiltrates in the tumor microenvironment (31). *C3AR1* upregulation was recently reported to correlate with chemoresistance and the survival of patients with soft tissue sarcoma (32). Using weighted gene co-expression network analysis, Pan *et al.* also identified several immune inflammatory response-related genes (including *C3AR1*) in GBM, particularly in the mesenchymal subtype (33). It has been proposed that *C3aR1* is upregulated in response to RT, which affects RT-induced tumor-specific immunity (34).

One limitation of our study was that our research was

retrospective. Therefore, prospective studies are needed to confirm our results. In addition, the gene signatures were analyzed based on TCGA and CGGA data, and these findings should be verified in clinical, cellular, and animal experiments.

## Conclusions

In conclusion, using the ESTIMATE algorithm, our bioinformatics analysis of patients with GBM-RT enabled the identification of GBM microenvironment-related genes associated with radioresistance. The stromal/immune score-based gene signatures identified here represent promising biomarkers for GBM and provide a theoretical basis for predicting the radioresponses and clinical outcomes of patients with GBM. However, further investigation is necessary to examine potential associations between these genes and RT combined with immunotherapy.

## Acknowledgments

*Funding:* This work was supported by the Fundamental Research Funds for the Central Universities (grant numbers WK9110000131).

## Footnote

*Reporting Checklist:* The authors have completed the MDAR checklist. Available at <http://dx.doi.org/10.21037/tcr-20-2476>

*Peer Review File:* Available at <http://dx.doi.org/10.21037/tcr-20-2476>

*Conflicts of Interest:* All authors have completed the ICMJE uniform disclosure form (available at <http://dx.doi.org/10.21037/tcr-20-2476>). The authors have no conflicts of interest to declare.

*Ethical Statement:* The authors are accountable for all aspects of the work in ensuring that questions related to the accuracy or integrity of any part of the work are appropriately investigated and resolved. The study was conducted in accordance with the Declaration of Helsinki (as revised in 2013).

*Open Access Statement:* This is an Open Access article distributed in accordance with the Creative Commons Attribution-NonCommercial-NoDerivs 4.0 International License (CC BY-NC-ND 4.0), which permits the non-

commercial replication and distribution of the article with the strict proviso that no changes or edits are made and the original work is properly cited (including links to both the formal publication through the relevant DOI and the license). See: <https://creativecommons.org/licenses/by-nc-nd/4.0/>.

## References

1. Stupp R, Mason WP, van den Bent MJ, et al. Radiotherapy plus concomitant and adjuvant temozolomide for glioblastoma. *N Engl J Med* 2005;352:987-96.
2. Urbańska K, Sokołowska J, Szmidt M, et al. Glioblastoma multiforme - an overview. *Contemp Oncol (Pozn)* 2014;18:307-12.
3. Gupta K, Burns TC. Radiation-induced alterations in the recurrent glioblastoma microenvironment: therapeutic implications. *Front Oncol* 2018;8:503.
4. Zhang H, Zhou Y, Cui B, et al. Novel insights into astrocyte-mediated signaling of proliferation, invasion and tumor immune microenvironment in glioblastoma. *Biomed Pharmacother* 2020;126:110086.
5. Quail DF, Joyce JA. The microenvironmental landscape of brain tumors. *Cancer Cell* 2017;31:326-41.
6. Zhu W, Xie L, Han J, et al. The application of deep learning in cancer prognosis prediction. *Cancers (Basel)* 2020;12:603.
7. Yoshihara K, Shahmoradgoli M, Martínez E, et al. Inferring tumour purity and stromal and immune cell admixture from expression data. *Nat Commun* 2013;4:2612.
8. Jia D, Li S, Li D, et al. Mining TCGA database for genes of prognostic value in glioblastoma microenvironment. *Aging (Albany NY)* 2018;10:592-605.
9. Bi KW, Wei XG, Qin XX, et al. BTK has potential to be a prognostic factor for lung adenocarcinoma and an indicator for tumor microenvironment remodeling: a study based on TCGA data mining. *Front Oncol* 2020;10:424.
10. Wang H, Wu X, Chen Y. Stromal-immune score-based gene signature: a prognosis stratification tool in gastric cancer. *Front Oncol* 2019;9:1212.
11. Ritchie ME, Phipson B, Wu D, et al. limma powers differential expression analyses for RNA-sequencing and microarray studies. *Nucleic Acids Res* 2015;43:e47.
12. Lin G, Chai J, Yuan S, C. et al. VennPainter: a tool for the comparison and identification of candidate genes based on Venn diagrams. *PLoS One* 2016;11:e0154315.
13. Shannon P, Markiel A, Ozier O, et al. Cytoscape: a software environment for integrated models of

- biomolecular interaction networks. *Genome Res* 2003;13:2498-504.
14. Stapleton S, Jaffray D, Milosevic M. Radiation effects on the tumor microenvironment: Implications for nanomedicine delivery. *Adv Drug Deliv Rev* 2017;109:119-30.
  15. Rath BH, Wahba A, Camphausen K, et al. Coculture with astrocytes reduces the radiosensitivity of glioblastoma stem-like cells and identifies additional targets for radiosensitization. *Cancer Med* 2015;4:1705-16.
  16. Hide T, Shibahara I, Kumabe T. Novel concept of the border niche: glioblastoma cells use oligodendrocytes progenitor cells (GAOs) and microglia to acquire stem cell-like features. *Brain Tumor Pathol* 2019;36:63-73.
  17. Dahan P, Martinez Gala J, Delmas C, et al. Ionizing radiations sustain glioblastoma cell dedifferentiation to a stem-like phenotype through survivin: possible involvement in radioresistance. *Cell Death Dis* 2014;5:e1543.
  18. Ramos RN, Rodriguez C, Hubert M, et al. CD163+ tumor-associated macrophage accumulation in breast cancer patients reflects both local differentiation signals and systemic skewing of monocytes. *Clin Transl Immunology* 2020;9:e1108.
  19. Yu Y, Ke L, Lv X, et al. The prognostic significance of carcinoma-associated fibroblasts and tumor-associated macrophages in nasopharyngeal carcinoma. *Cancer Manag Res* 2018;10:1935-46.
  20. Garvin S, Oda H, Arnesson LG, et al. Tumor cell expression of CD163 is associated to postoperative radiotherapy and poor prognosis in patients with breast cancer treated with breast-conserving surgery. *J Cancer Res Clin Oncol* 2018;144:1253-63.
  21. Chen T, Chen J, Zhu Y, et al. CD163, a novel therapeutic target, regulates the proliferation and stemness of glioma cells via casein kinase 2. *Oncogene* 2019;38:1183-99.
  22. Vidyarthi A, Agnihotri T, Khan N, et al. Predominance of M2 macrophages in gliomas leads to the suppression of local and systemic immunity. *Cancer Immunol Immunother* 2019;68:1995-2004.
  23. Leblond MM, Pérès EA, Helaine C, et al. M2 macrophages are more resistant than M1 macrophages following radiation therapy in the context of glioblastoma. *Oncotarget* 2017;8:72597-612.
  24. Liu YD, Yu L, Ying L, et al. Toll-like receptor 2 regulates metabolic reprogramming in gastric cancer via superoxide dismutase 2. *Int J Cancer* 2019;144:3056-69.
  25. Zhao S, Zhang Y, Zhang Q, et al. Toll-like receptors and prostate cancer. *Front Immunol* 2014;5:352.
  26. Semlali A, Parine NR, Al-Numair NS, et al. Potential role of Toll-like receptor 2 expression and polymorphisms in colon cancer susceptibility in the Saudi Arabian population. *Onco Targets Ther* 2018;11:8127-41.
  27. Qian J, Luo F, Yang J, et al. TLR2 promotes glioma immune evasion by downregulating MHC class II molecules in microglia. *Cancer Immunol Res* 2018;6:1220-33.
  28. Li C, Ma L, Liu Y, et al. TLR2 promotes development and progression of human glioma via enhancing autophagy. *Gene* 2019;700:52-9.
  29. Gao F, Zhang C, Zhou C, et al. A critical role of toll-like receptor 2 (TLR2) and its' in vivo ligands in radioresistance. *Sci Rep* 2015;5:13004.
  30. Chang CY, Jeon SB, Yoon HJ, et al. Glial TLR2-driven innate immune responses and CD8+ T cell activation against brain tumor. *Glia* 2019;67:1179-95.
  31. Sayegh ET, Bloch O, Parsa AT. Complement anaphylatoxins as immune regulators in cancer. *Cancer Med* 2014;3:747-58.
  32. Zhang J, Chen M, Zhao Y, et al. Complement and coagulation cascades pathway correlates with chemosensitivity and overall survival in patients with soft tissue sarcoma. *Eur J Pharmacol* 2020;879:173121.
  33. Pan YB, Wang S, Yang B, et al. Transcriptome analyses reveal molecular mechanisms underlying phenotypic differences among transcriptional subtypes of glioblastoma. *J Cell Mol Med* 2020;24:3901-16.
  34. Surace L, Lysenko V, Fontana AO, et al. Complement Is a central mediator of radiotherapy-induced tumor-specific immunity and clinical response. *Immunity* 2015;42:767-77.

**Cite this article as:** Liu Y, Zhao Y, Fang J, Fang J, Yuan X. Bioinformatics analysis of microenvironment-related genes associated with radioresistance in glioblastoma. *Transl Cancer Res* 2020;9(12):7495-7504. doi: 10.21037/tcr-20-2476

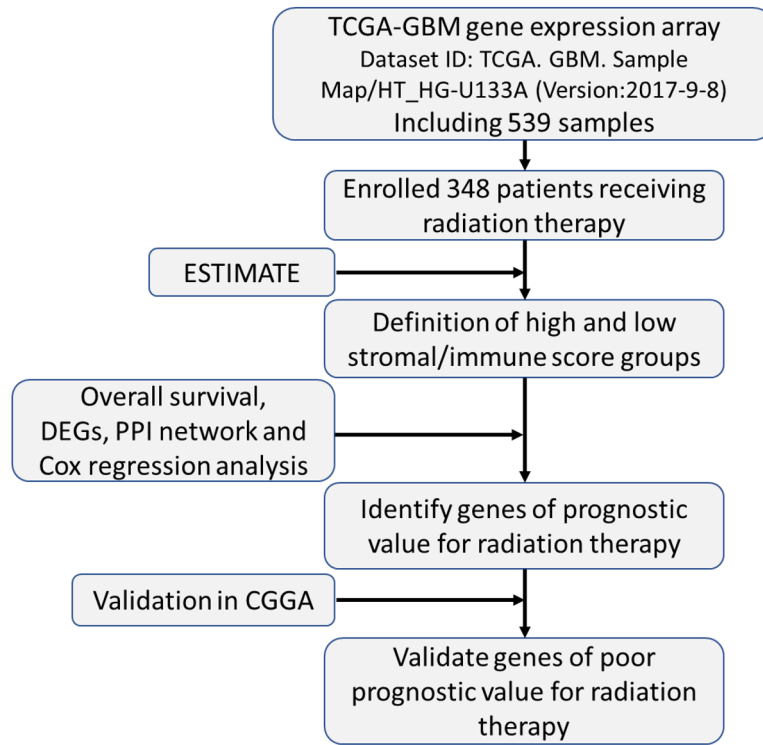


**Figure S1** Analysis workflow of the current study.

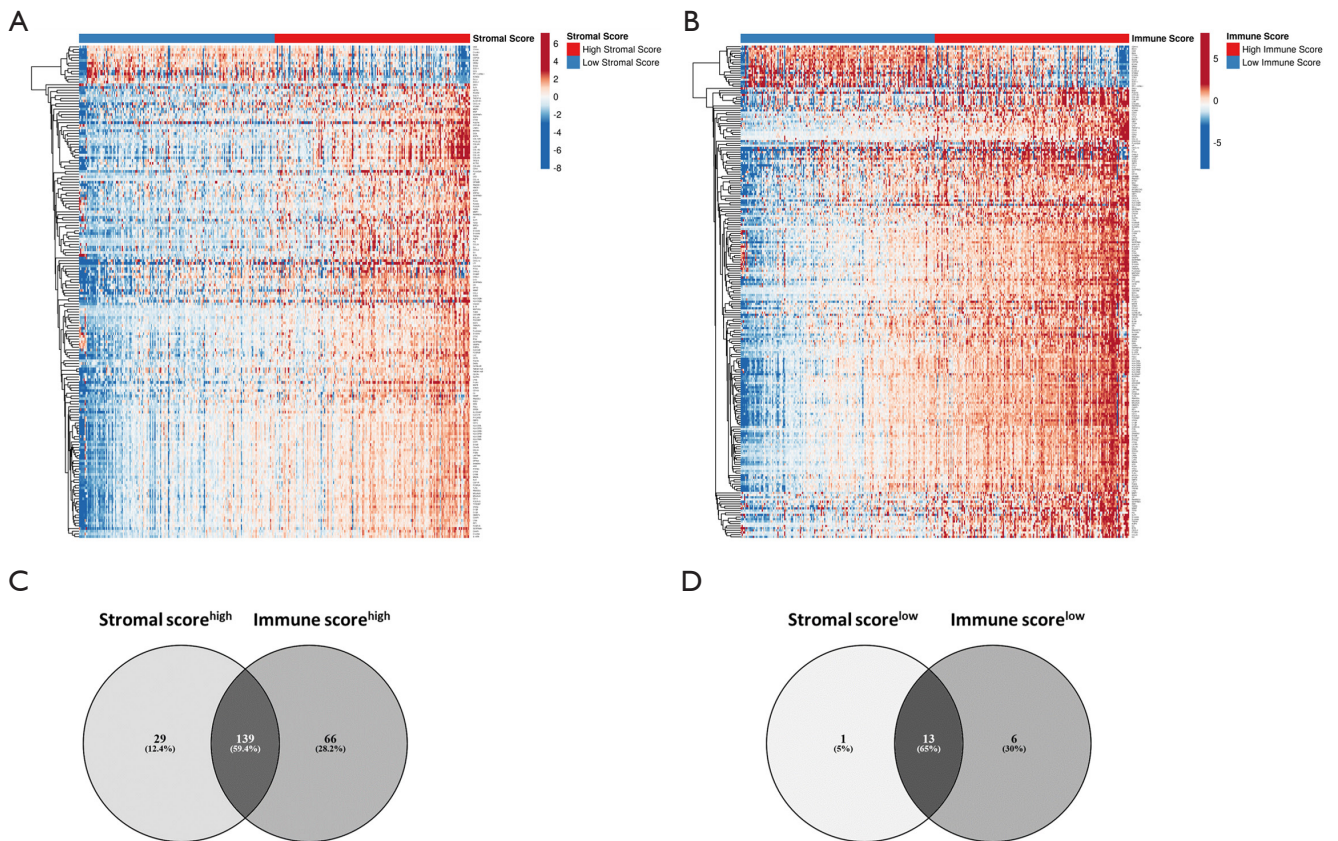


**Figure S2** Differential analysis of gene-expression profiles related to stromal and immune scores in patients with GBM-RT. (A,B) Heatmap for DEGs generated by comparing groups with (A) high and low stromal score groups, and (B) groups with high and low immune score. DEGs were determined using the limma package of R software, with the criteria of  $P < 0.05$  and  $|\log_2 \text{fold-change}| > 1$ . (C,D) Venn diagrams of intersecting DEGs in groups with high or low stromal/immune scores.

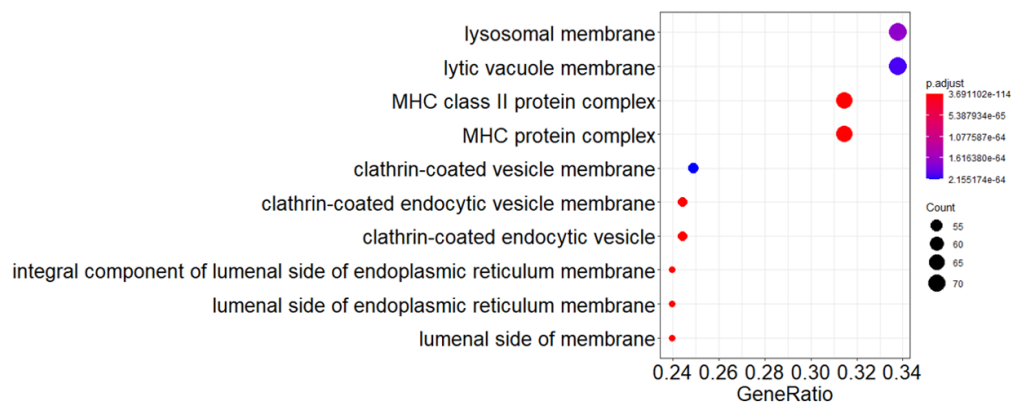


**Figure S3** GO-based enrichment analysis of 139 DEGs in term of CCs.

**Table S1** Top 20 GO terms of biological process

Ontology	ID	Description	GeneRatio	pvalue	p.adjust	qvalue	Count
BP	GO:0002495	Antigen processing and presentation of peptide antigen via MHC class II	72/207	2.22E-98	4.52E-95	3.28E-95	72
BP	GO:0002504	Antigen processing and presentation of peptide or polysaccharide antigen via MHC class II	72/207	3.59E-98	4.52E-95	3.28E-95	72
BP	GO:0019886	Antigen processing and presentation of exogenous peptide antigen via MHC class II	71/207	4.92E-97	4.13E-94	3.00E-94	71
BP	GO:0048002	Antigen processing and presentation of peptide antigen	76/207	5.37E-82	3.38E-79	2.45E-79	76
BP	GO:0002478	Antigen processing and presentation of exogenous peptide antigen	75/207	7.73E-82	3.89E-79	2.82E-79	75
BP	GO:0019884	Antigen processing and presentation of exogenous antigen	75/207	4.28E-81	1.79E-78	1.30E-78	75
BP	GO:0019882	Antigen processing and presentation	77/207	1.42E-79	5.11E-77	3.71E-77	77
BP	GO:0034341	Response to interferon-gamma	73/207	1.43E-78	4.50E-76	3.27E-76	73
BP	GO:0071346	Cellular response to interferon-gamma	66/207	6.76E-70	1.89E-67	1.37E-67	66
BP	GO:0060333	Interferon-gamma-mediated signaling pathway	54/207	6.00E-63	1.51E-60	1.10E-60	54
BP	GO:0050852	T cell receptor signaling pathway	52/207	5.45E-50	1.25E-47	9.06E-48	52
BP	GO:0050851	Antigen receptor-mediated signaling pathway	54/207	5.70E-49	1.20E-46	8.68E-47	54
BP	GO:0002399	MHC class II protein complex assembly	23/207	3.42E-47	6.15E-45	4.46E-45	23
BP	GO:0002503	Peptide antigen assembly with MHC class II protein complex	23/207	3.42E-47	6.15E-45	4.46E-45	23
BP	GO:0002501	Peptide antigen assembly with MHC protein complex	23/207	1.01E-44	1.69E-42	1.23E-42	23
BP	GO:0002396	MHC protein complex assembly	23/207	6.55E-41	1.03E-38	7.48E-39	23
BP	GO:0042102	Positive regulation of T cell proliferation	36/207	8.13E-41	1.20E-38	8.74E-39	36
BP	GO:0050671	Positive regulation of lymphocyte proliferation	37/207	2.18E-38	3.05E-36	2.21E-36	37
BP	GO:0032946	Positive regulation of mononuclear cell proliferation	37/207	2.73E-38	3.62E-36	2.63E-36	37
BP	GO:0070663	Regulation of leukocyte proliferation	43/207	1.44E-37	1.81E-35	1.31E-35	43

**Table S2** Top 20 GO terms of molecular function (MF)

Ontology	ID	Description	GeneRatio	pvalue	p.adjust	qvalue	Count
MF	GO:0042605	Peptide antigen binding	50/208	1.03E-68	3.02E-66	2.42E-66	50
MF	GO:0032395	MHC class II receptor activity	36/208	2.20E-56	3.24E-54	2.59E-54	36
MF	GO:0003823	Antigen binding	50/208	5.31E-56	5.22E-54	4.17E-54	50
MF	GO:0042277	Peptide binding	56/208	2.26E-46	1.67E-44	1.33E-44	56
MF	GO:0023026	MHC class II protein complex binding	30/208	3.09E-46	1.82E-44	1.46E-44	30
MF	GO:0033218	Amide binding	57/208	3.34E-44	1.64E-42	1.31E-42	57
MF	GO:0023023	MHC protein complex binding	30/208	2.36E-41	9.96E-40	7.96E-40	30
MF	GO:0140375	Immune receptor activity	44/208	6.29E-40	2.32E-38	1.85E-38	44
MF	GO:0030247	Polysaccharide binding	15/208	6.36E-21	2.08E-19	1.67E-19	15
MF	GO:0030246	Carbohydrate binding	19/208	4.48E-10	1.32E-08	1.06E-08	19
MF	GO:0061134	Peptidase regulator activity	17/208	1.21E-09	3.23E-08	2.58E-08	17
MF	GO:0004866	Endopeptidase inhibitor activity	15/208	3.66E-09	9.00E-08	7.19E-08	15
MF	GO:0030414	Peptidase inhibitor activity	15/208	5.86E-09	1.33E-07	1.06E-07	15
MF	GO:0061135	Endopeptidase regulator activity	15/208	6.67E-09	1.41E-07	1.12E-07	15
MF	GO:0070628	Proteasome binding	7/208	1.71E-08	3.37E-07	2.69E-07	7
MF	GO:0004867	Serine-type endopeptidase inhibitor activity	10/208	1.07E-07	1.97E-06	1.57E-06	10
MF	GO:0008009	Chemokine activity	8/208	3.22E-07	5.58E-06	4.46E-06	8
MF	GO:0019864	IgG binding	4/208	2.43E-06	3.98E-05	3.18E-05	4
MF	GO:0035325	Toll-like receptor binding	4/208	5.63E-06	8.74E-05	6.98E-05	4
MF	GO:0042379	Chemokine receptor binding	8/208	5.95E-06	8.77E-05	7.01E-05	8

**Table S3** Top 20 GO terms of cellular components

Ontology	ID	Description	GeneRatio	pvalue	p.adjust	qvalue	Count
CC	GO:0042613	MHC class II protein complex	67/213	2.38E-116	3.69E-114	2.03E-114	67
CC	GO:0042611	MHC protein complex	67/213	2.96E-99	2.30E-97	1.26E-97	67
CC	GO:0030669	Clathrin-coated endocytic vesicle membrane	52/213	3.26E-79	1.68E-77	9.26E-78	52
CC	GO:0045334	Clathrin-coated endocytic vesicle	52/213	1.76E-73	6.81E-72	3.74E-72	52
CC	GO:0071556	Integral component of luminal side of endoplasmic reticulum membrane	51/213	2.35E-70	6.07E-69	3.34E-69	51
CC	GO:0098553	Luminal side of endoplasmic reticulum membrane	51/213	2.35E-70	6.07E-69	3.34E-69	51
CC	GO:0098576	Luminal side of membrane	51/213	4.53E-69	1.00E-67	5.52E-68	51
CC	GO:0005765	Lysosomal membrane	72/213	8.71E-66	1.69E-64	9.29E-65	72
CC	GO:0098852	Lytic vacuole membrane	72/213	1.19E-65	2.06E-64	1.13E-64	72
CC	GO:0030665	Clathrin-coated vesicle membrane	53/213	1.39E-65	2.16E-64	1.19E-64	53
CC	GO:0030134	COPII-coated ER to Golgi transport vesicle	54/213	1.59E-65	2.24E-64	1.23E-64	54
CC	GO:0012507	ER to Golgi transport vesicle membrane	51/213	2.82E-65	3.64E-64	2.00E-64	51
CC	GO:0032588	Trans-Golgi network membrane	51/213	1.36E-64	1.62E-63	8.91E-64	51
CC	GO:0030666	Endocytic vesicle membrane	58/213	1.99E-60	2.20E-59	1.21E-59	58
CC	GO:0030660	Golgi-associated vesicle membrane	51/213	2.09E-57	2.16E-56	1.19E-56	51
CC	GO:0030136	Clathrin-coated vesicle	53/213	5.25E-56	5.09E-55	2.80E-55	53
CC	GO:0005798	Golgi-associated vesicle	54/213	3.85E-55	3.51E-54	1.93E-54	54
CC	GO:0030662	Coated vesicle membrane	53/213	1.54E-53	1.32E-52	7.27E-53	53
CC	GO:0030139	Endocytic vesicle	61/213	1.81E-53	1.47E-52	8.11E-53	61
CC	GO:0030176	Integral component of endoplasmic reticulum membrane	51/213	6.62E-51	5.13E-50	2.82E-50	51

**Table S4** Enrichment of KEGG pathways

ID	Description	GeneRatio	pvalue	p.adjust	qvalue	Count
hsa05150	Staphylococcus aureus infection	20/88	7.12E-21	1.00E-18	6.30E-19	20
hsa05152	Tuberculosis	22/88	1.19E-17	8.37E-16	5.25E-16	22
hsa05140	Leishmaniasis	16/88	8.32E-17	3.54E-15	2.22E-15	16
hsa04145	Phagosome	20/88	1.00E-16	3.54E-15	2.22E-15	20
hsa04610	Complement and coagulation cascades	15/88	1.11E-14	3.12E-13	1.96E-13	15
hsa05323	Rheumatoid arthritis	15/88	4.49E-14	1.05E-12	6.61E-13	15
hsa05332	Graft-versus-host disease	10/88	1.63E-11	3.28E-10	2.06E-10	10
hsa05310	Asthma	9/88	2.48E-11	4.37E-10	2.74E-10	9
hsa04640	Hematopoietic cell lineage	13/88	3.79E-11	5.95E-10	3.73E-10	13
hsa05321	Inflammatory bowel disease (IBD)	11/88	7.94E-11	1.12E-09	7.02E-10	11
hsa05322	Systemic lupus erythematosus	14/88	1.79E-10	2.30E-09	1.44E-09	14
hsa05133	Pertussis	11/88	4.61E-10	5.42E-09	3.40E-09	11
hsa04612	Antigen processing and presentation	11/88	6.15E-10	6.27E-09	3.93E-09	11
hsa04940	Type I diabetes mellitus	9/88	6.23E-10	6.27E-09	3.93E-09	9
hsa04672	Intestinal immune network for IgA production	9/88	2.15E-09	2.02E-08	1.27E-08	9
hsa05145	Toxoplasmosis	12/88	2.51E-09	2.22E-08	1.39E-08	12
hsa05164	Influenza A	14/88	3.49E-09	2.89E-08	1.82E-08	14
hsa05330	Allograft rejection	8/88	5.62E-09	4.40E-08	2.76E-08	8
hsa04061	Viral protein interaction with cytokine and cytokine receptor	11/88	9.22E-09	6.84E-08	4.29E-08	11
hsa05416	Viral myocarditis	9/88	1.40E-08	9.90E-08	6.21E-08	9
hsa05320	Autoimmune thyroid disease	8/88	8.91E-08	5.98E-07	3.75E-07	8
hsa05134	Legionellosis	8/88	1.60E-07	1.03E-06	6.44E-07	8
hsa04659	Th17 cell differentiation	10/88	2.18E-07	1.34E-06	8.39E-07	10
hsa04668	TNF signaling pathway	10/88	3.36E-07	1.98E-06	1.24E-06	10
hsa04514	Cell adhesion molecules (CAMs)	11/88	5.43E-07	3.06E-06	1.92E-06	11
hsa04657	IL-17 signaling pathway	9/88	7.46E-07	4.05E-06	2.54E-06	9
hsa05169	Epstein-Barr virus infection	12/88	1.68E-06	8.78E-06	5.50E-06	12
hsa04658	Th1 and Th2 cell differentiation	8/88	6.61E-06	3.33E-05	2.09E-05	8
hsa04933	AGE-RAGE signaling pathway in diabetic complications	8/88	1.23E-05	5.99E-05	3.75E-05	8
hsa05142	Chagas disease (American trypanosomiasis)	8/88	1.43E-05	6.48E-05	4.06E-05	8
hsa05146	Amoebiasis	8/88	1.43E-05	6.48E-05	4.06E-05	8
hsa05144	Malaria	6/88	1.57E-05	6.84E-05	4.29E-05	6
hsa04064	NF-kappa B signaling pathway	8/88	1.64E-05	6.84E-05	4.29E-05	8
hsa04060	Cytokine-cytokine receptor interaction	13/88	1.65E-05	6.84E-05	4.29E-05	13
hsa05166	Human T-cell leukemia virus 1 infection	11/88	2.43E-05	9.81E-05	6.15E-05	11
hsa04620	Toll-like receptor signaling pathway	7/88	0.000134	0.000524	0.000329	7
hsa05168	Herpes simplex virus 1 infection	15/88	0.000252	0.00096	0.000602	15
hsa05132	Salmonella infection	9/88	0.000398	0.001479	0.000927	9
hsa04380	Osteoclast differentiation	7/88	0.000482	0.001741	0.001092	7
hsa05020	Prion diseases	4/88	0.000543	0.001915	0.001201	4
hsa04621	NOD-like receptor signaling pathway	8/88	0.000787	0.002706	0.001697	8
hsa04062	Chemokine signaling pathway	8/88	0.001043	0.003501	0.002195	8
hsa04666	Fc gamma R-mediated phagocytosis	5/88	0.003433	0.011258	0.00706	5
hsa04210	Apoptosis	6/88	0.00367	0.011759	0.007374	6
hsa01523	Antifolate resistance	3/88	0.004575	0.014336	0.00899	3
hsa04623	Cytosolic DNA-sensing pathway	4/88	0.004898	0.015014	0.009415	4
hsa04625	C-type lectin receptor signaling pathway	5/88	0.005532	0.016595	0.010407	5
hsa05221	Acute myeloid leukemia	4/88	0.006098	0.017912	0.011233	4
hsa05143	African trypanosomiasis	3/88	0.007544	0.021709	0.013614	3
hsa04217	Necroptosis	6/88	0.007804	0.022008	0.013801	6
hsa04611	Platelet activation	5/88	0.011428	0.031596	0.019814	5
hsa05135	Yersinia infection	5/88	0.01381	0.037446	0.023482	5
hsa05167	Kaposi sarcoma-associated herpesvirus infection	6/88	0.017255	0.045636	0.028618	6
hsa05162	Measles	5/88	0.017477	0.045636	0.028618	5
hsa05130	Pathogenic Escherichia coli infection	6/88	0.018505	0.046593	0.029218	6
hsa05202	Transcriptional misregulation in cancer	6/88	0.018505	0.046593	0.029218	6

**Table S5** Correlation of the selected DEGs with the OS of patients with GBM-RT identified by Cox regression analysis in TCGA database

Terms	HR[exp(coef)]	coef	95% CI lower	95% CI upper	Z	P value
DLL3	0.881408	-0.12623	-0.19726	-0.05521	-3.48372	4.94E-04
BCAN	0.917235	-0.08639	-0.16807	-0.00471	-2.07305	0.038167
PLA2G2A	1.051875	0.050574	6.10E-04	0.100539	1.983877	0.04727
LTF	1.056815	0.055259	0.017223	0.093295	2.847469	0.004407
SLPI	1.060782	0.059006	0.005916	0.112097	2.178359	0.029379
CXCL10	1.064471	0.062478	0.002551	0.122406	2.04338	0.041015
COL6A3	1.065954	0.063871	0.011623	0.116118	2.395979	0.016576
FCGBP	1.068699	0.066442	0.005769	0.127116	2.146339	0.031846
PI3	1.073327	0.070763	0.005245	0.136282	2.116854	0.034272
LYZ	1.073906	0.071302	0.007092	0.135512	2.176429	0.029523
VSIG4	1.075443	0.072733	0.002282	0.143183	2.02346	0.043026
IL8	1.075938	0.073192	0.007456	0.138929	2.182266	0.02909
TREM1	1.07641	0.073631	0.002621	0.144642	2.032294	0.042124
CHI3L2	1.077258	0.074419	0.019478	0.129359	2.65483	0.007935
CXCL14	1.080297	0.077236	0.030698	0.123773	3.252858	0.001143
GPNMB	1.082401	0.079181	0.012482	0.145881	2.326751	0.019979
NNMT	1.08533	0.081884	0.030996	0.132773	3.153747	0.001612
POSTN	1.087824	0.084179	0.044279	0.124079	4.134989	3.55E-05
ALOX5AP	1.08895	0.085214	0.013445	0.156983	2.327134	0.019958
SERPINA1	1.090036	0.086211	0.013712	0.15871	2.330656	0.019772
CCL20	1.090169	0.086333	0.007298	0.165368	2.140943	0.032279
CHI3L1	1.091505	0.087558	0.040746	0.134369	3.665969	2.46E-04
F13A1	1.091961	0.087975	0.028615	0.147335	2.904795	0.003675
TNFSF10	1.092109	0.08811	0.002294	0.173927	2.012352	0.044183
RGS1	1.093359	0.089254	0.015567	0.162941	2.374022	0.017595
HLA-DMA	1.094432	0.090236	0.001664	0.178807	1.996796	0.045847
C1QA	1.095929	0.091603	0.01	0.173206	2.200141	0.027797
CP	1.099548	0.094899	0.026501	0.163298	2.719338	0.006541
SAMSN1	1.100264	0.09555	0.003059	0.188041	2.024793	0.042889
CD163	1.100454	0.095723	0.03367	0.157775	3.02344	0.002499
AIM1	1.106014	0.100762	0.02152	0.180005	2.492221	0.012695
RNASE1	1.107058	0.101706	0.018785	0.184627	2.403972	0.016218
SOD2	1.107097	0.101741	0.009082	0.194401	2.152062	0.031392
FCER1G	1.108624	0.10312	0.018343	0.187897	2.384032	0.017124
PTX3	1.109612	0.10401	0.04603	0.16199	3.515971	4.38E-04
BIRC3	1.110015	0.104373	0.012755	0.195991	2.232831	0.02556
CCL2	1.110579	0.104882	0.046226	0.163537	3.504605	4.57E-04
UBD	1.112426	0.106543	0.031787	0.1813	2.793343	0.005217
BCL2A1	1.113078	0.10713	0.02548	0.188779	2.571606	0.010123
CLEC2B	1.115707	0.109488	0.02679	0.192186	2.594891	0.009462
S100A4	1.116046	0.109792	0.036712	0.182873	2.944552	0.003234
LY96	1.116715	0.110391	0.026205	0.194577	2.570053	0.010168
C3AR1	1.118796	0.112254	0.008528	0.215979	2.121106	0.033913
FCGR1A	1.119057	0.112487	0.008706	0.216267	2.124384	0.033638
DPYD	1.121302	0.114491	0.036672	0.19231	2.883576	0.003932
S100A8	1.121341	0.114526	0.043056	0.185995	3.14072	0.001685
CTSS	1.121415	0.114592	0.017865	0.211318	2.321973	0.020234
CCR1	1.122064	0.11517	8.94E-04	0.229446	1.975298	0.048234
CD14	1.125668	0.118376	0.036756	0.199997	2.842593	0.004475
LAPTM5	1.128666	0.121036	0.022499	0.219574	2.407486	0.016063
ITGB2	1.130141	0.122342	0.025103	0.219581	2.465937	0.013666
FLJ22662	1.130952	0.12306	0.026339	0.219781	2.493702	0.012642
PYCARD	1.131215	0.123292	0.016127	0.230457	2.254916	0.024139
IL10RA	1.131224	0.1233	0.023577	0.223023	2.423355	0.015378
IL1B	1.131917	0.123913	0.027372	0.220454	2.515673	0.011881
SERPINE1	1.132382	0.124323	0.046999	0.201648	3.15127	0.001626
TGFBI	1.132835	0.124723	0.044614	0.204832	3.051493	0.002277
CXorf9	1.133711	0.125496	0.016541	0.234452	2.257518	0.023976
PTPRC	1.135169	0.126782	0.028047	0.225517	2.516718	0.011845
C1orf38	1.135762	0.127304	0.013093	0.241514	2.184654	0.028914
RNASE6	1.13619	0.127681	0.027556	0.227806	2.49937	0.012441
CFI	1.13753	0.128859	0.049446	0.208272	3.180315	0.001471
S100A9	1.139868	0.130912	0.054232	0.207592	3.346154	8.19E-04
SERPINF1	1.140222	0.131223	0.045693	0.216753	3.007054	0.002638
SQRDL	1.141299	0.132167	0.032157	0.232177	2.590175	0.009593
CLEC7A	1.143047	0.133698	0.017518	0.249878	2.255491	0.024103
TLR2	1.145966	0.136248	0.031434	0.241062	2.547769	0.010841
SLA	1.147324	0.137432	0.037735	0.237129	2.70181	0.006896
PSCDBP	1.147956	0.137983	0.033347	0.242618	2.584608	0.009749
FGL2	1.149974	0.139739	0.021932	0.257547	2.324849	0.02008
GPR65	1.151432	0.141006	0.032105	0.249908	2.537767	0.011156
CSTA	1.153006	0.142373	0.066494	0.218251	3.677507	2.36E-04
IFI30	1.153156	0.142503	0.046641	0.238365	2.913577	0.003573
C1S	1.15346	0.142766	0.067038	0.218494	3.695023	2.20E-04
CECR1	1.155062	0.144154	0.051433	0.236875	3.04717	0.00231
C5AR1	1.158813	0.147396	0.046884	0.247909	2.874177	0.004051
NCF2	1.159058	0.147608	0.043079	0.252136	2.767728	0.005645
FCGR2B	1.159292	0.147809	0.074332	0.221286	3.942732	8.06E-05
FCGR2A	1.159377	0.147883	0.048799	0.246967	2.925244	0.003442
SERPING1	1.159456	0.147951	0.072158	0.223745	3.82592	1.30E-04
TMEM176B	1.159545	0.148028	0.067693	0.228362	3.611518	3.04E-04
TNFAIP3	1.161278	0.149521	0.029151	0.269891	2.434619	0.014907
CSF2RB	1.161308	0.149547	0.024369	0.274724	2.341523	0.019205
STAB1	1.161958	0.150106	0.046476	0.253737	2.838965	0.004526
RNASE2	1.162077	0.150209	0.057075	0.243344	3.16107	0.001572
CYBB	1.171486	0.158273	0.038136	0.278411	2.582118	0.00982
SERPINB1	1.180691	0.1661	0.069733	0.262467	3.378224	7.30E-04
PLAUR	1.220504	0.199264	0.084103	0.314426	3.391329	6.96E-04

OS, overall survival in terms of days.

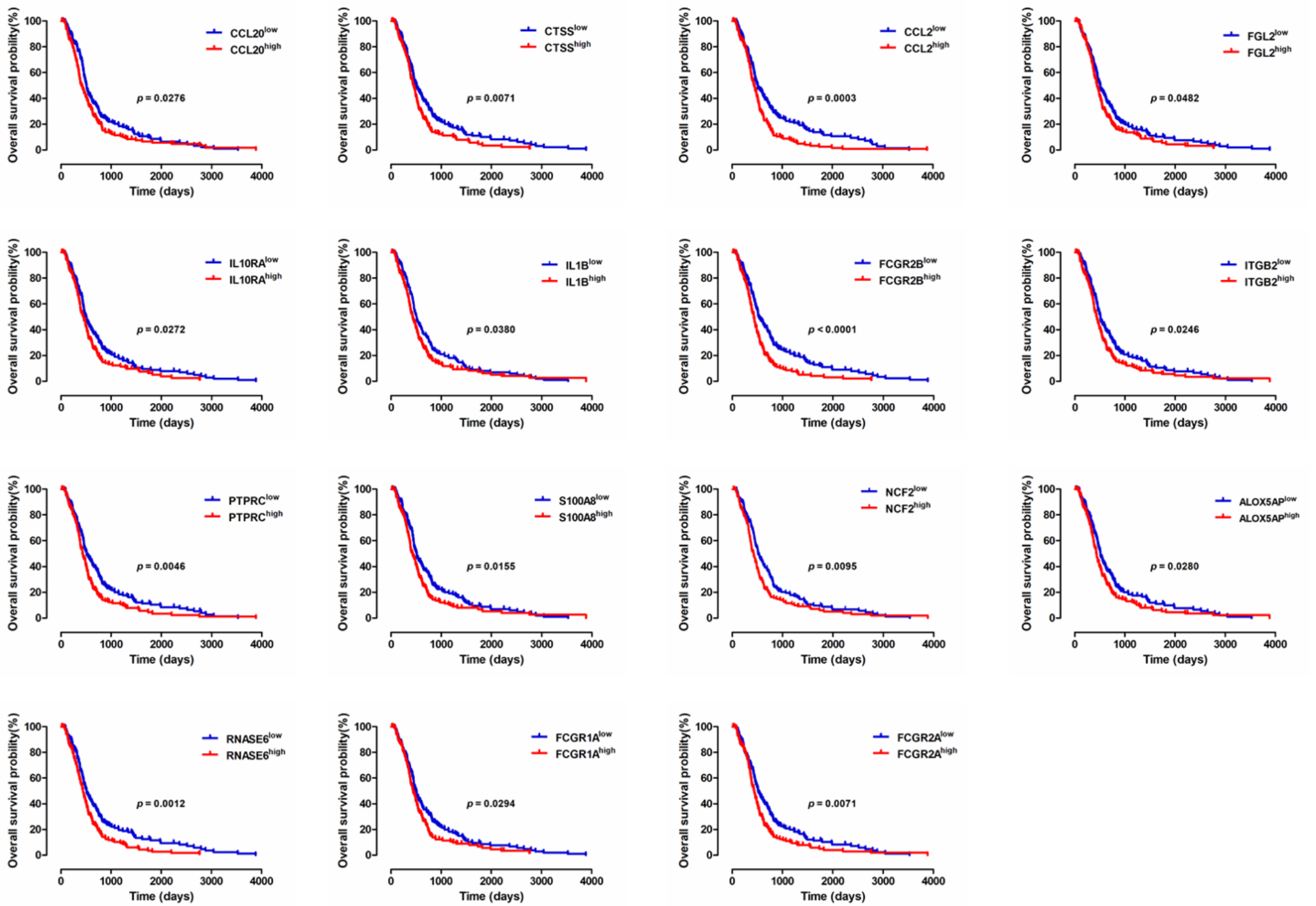


**Figure S4** Correlation of the selected DEGs with the OS of patients in TCGA database. Survival analysis was conducted by generating Kaplan-Meier curves. DEGs were grouped based on high (red line, n=174) or low (blue line, n=174) expression levels relative to the median gene-expression level. P<0.05, as determined by the log-rank test. OS, overall survival in terms of days.

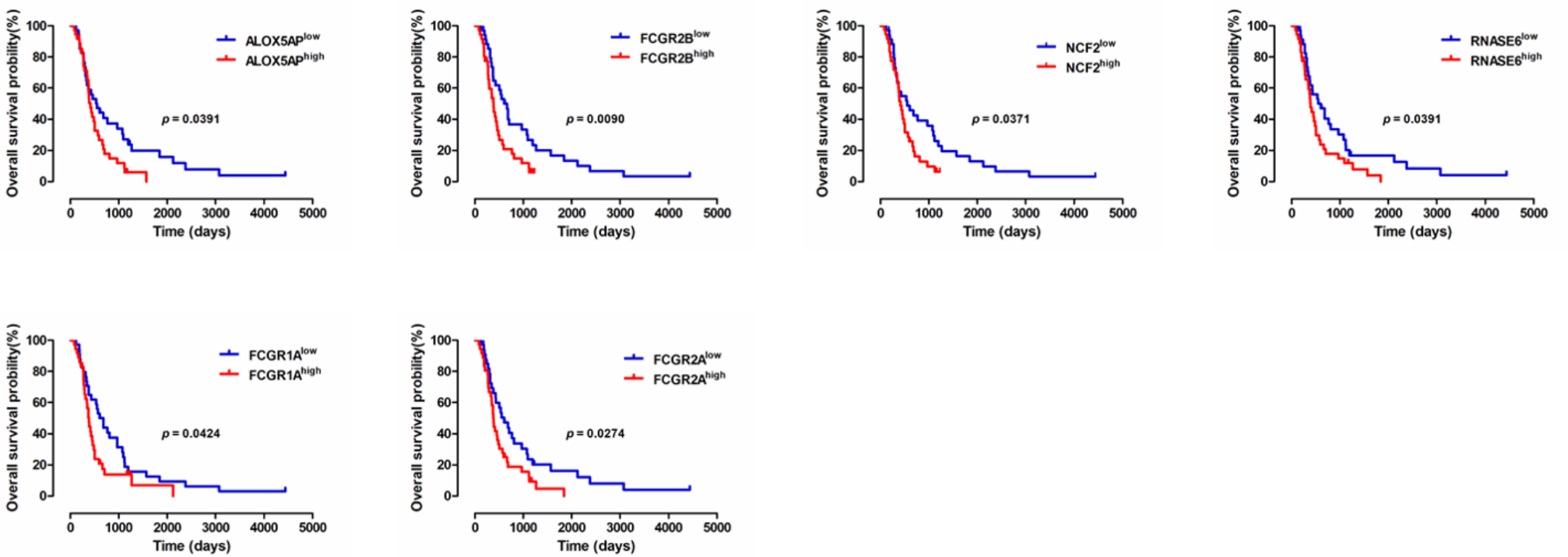


**Figure S5** Validation of the selected DEGs in the CGGA cohort. Survival analysis was conducted by generating Kaplan-Meier curves. DEGs were grouped based on high (red line, n=36) or low (blue line, n=35) expression levels relative to the median gene expression level. P<0.05, as determined by the log-rank test.